

K-shell Core Electron Excitations in Electronic Stopping of Protons in Water from First Principles

*Yi Yao, Dillon C. Yost, and Yosuke Kanai**

Department of Chemistry, University of North Carolina at Chapel Hill, North Carolina, 27599, USA

Understanding the role of core electron excitation in liquid water under proton irradiation has become important due to the growing use of proton beams in radiation oncology. Using a first-principles, non-equilibrium simulation approach based on real-time time-dependent density functional theory, we determine the electronic stopping power, the velocity-dependent energy transfer rate from irradiating ions to electrons. The electronic stopping power curve agrees quantitatively with experimental data over the velocity range available. At the same time, significant differences are observed between our first-principles result and commonly-used perturbation theoretic models. Excitations of the water molecules' oxygen core electrons are a crucial factor in determining the electronic stopping power curve beyond its maximum. The core electron contribution is responsible for as much as one-third of the stopping power at the high proton velocity of 8.0 a.u. (1.6 MeV). K-shell core electron excitations not only provide an additional channel for the energy transfer but they also significantly influence the valence electron excitations. In the excitation process, generated holes remain highly localized within a few angstroms around the irradiating proton path whereas electrons are excited away from the path. In spite of its great contribution to the stopping power, K-shell electrons play a rather minor role in terms of the excitation density; only 1% of the hole population comprises K-shell holes even at the high proton velocity of 8.0 a.u.. The excitation behavior revealed here is distinctly different from that of photon-based ionizing radiation such as X/ γ -rays.

When a highly energetic ion travels through and interacts with matter, its kinetic energy is transferred into the target material's electronic and nuclear subsystems. This energy loss of the projectile ion can arise from both elastic collisions with nuclei (nuclear stopping) and inelastic scattering events (electronic stopping). When the particle's kinetic energy is sufficiently large (on the order of ~ 10 keV per nucleon), the major contribution to the energy transfer comprises electronic stopping wherein the projectile ion induces massive electronic excitations in the target matter¹⁻². This electronic stopping phenomenon is at the heart of emerging ion beam cancer therapies. The use of proton beam radiation over more conventional radiation based on X/ γ -ray photons is often considered more effective because of the ion's distinct spatial energy deposition profile with a very sharp peak.³⁻⁴ By calibrating the initial kinetic energy of the protons, this energy deposition peak can be tuned to coincide with the location of the tumour. This energy deposition profile is largely determined by electronic stopping power, which measures the rate of energy transfer from the charged particle to electrons in matter per unit distance of the energetic particle's movement.^{1,5-7} The stopping power is a continuous function of the particle velocity, and the velocities near the maximum of the stopping power are responsible for the formation of the sharp energy

deposition peak for ions like protons. Because liquid water makes up the majority of matter in human cells, various models have been developed for the electronic stopping power in liquid water over the years⁸⁻¹⁶ including our earlier first-principles theory result¹⁷⁻¹⁸. At the same time, only limited experimental measurements exist near the stopping power maximum, and various theoretical models are currently used with empirically fitted parameters. Furthermore, unraveling the details of the excitation behavior in the electronic stopping process has become important. Proton radiation is generally considered as being similar to other types of ionizing radiation like X/ γ -ray photons, which undergo Compton scattering and also core electron excitation. However, the extent to which proton radiation excites valence and core electrons is not understood. Indeed, this is complicated by the fact that the ratio of valence to core electron excitations depends on the irradiating proton velocity. In radiation oncology, an empirical factor such as relative biological effectiveness is used to take into account differences between the proton radiation and X-ray photon radiation for convenience, but many now call for a better mechanistic understanding of the radiation at the molecular level¹⁹. In this Letter, we discuss the role of K-shell core electron excitations in liquid water under proton irradiation by accurately determining the electronic stopping power and simulating

* E-mail: ykanai@unc.edu

quantum dynamics of electronic excitations from first principles.

We apply our recently developed non-equilibrium dynamics simulation approach based on real-time time-dependent density functional theory (RT-TDDFT)^{17-18, 20-23} to simulate the non-perturbative response of the electronic system to a fast-moving projectile proton. In this approach, the electronic stopping power can be obtained from the rate of electronic energy change at different projectile proton velocities as discussed in our earlier work^{21,24}. We use our implementation of RT-TDDFT based on a planewave-pseudopotential (PW-PP) formalism^{20, 25} in the Qbox/Qb@ll code²⁶⁻²⁷. Simulating the 1s core (i.e. K-shell) electron excitations of oxygen atoms in this study requires us to go beyond several standard approximations typically used in the PW-PP formalism. The oxygen and hydrogen atoms in liquid water are described by all-electron pseudopotentials that are generated using the optimized Norm-Conserving Vanderbilt scheme²⁸⁻²⁹, for which multiple projectors are used for the explicit treatment of the 1s electrons of oxygen atoms in the simulation. The validity of the all-electron pseudopotentials was checked by calculating the core-level optical excitation spectrum of a single water molecule as shown in the Supplemental Material. Unlike previous RT-TDDFT studies of electronic stopping in which pseudopotentials are used for the projectile proton¹⁷⁻¹⁸, here we use a bare Coulomb potential for representing the proton because an accurate description of the K-shell core excitations is necessary, especially for large proton velocities (see Supplemental Material for details). Consequently, the use of a planewave kinetic energy cutoff of up to 250 Ry for expanding the Kohn-Sham wavefunctions was required, and an extrapolation was used for calculating the stopping power at high velocities (see Supplemental Material for details). We employed the PBE GGA approximation³⁰ for the exchange-correlation potential because we found that the use of the more advanced SCAN meta-GGA does not change the results³¹⁻³³ (Supplemental Material Fig. S7). The liquid water structure was generated by taking a snapshot after performing a 10 ns classical molecular dynamics simulation at 300K with SPC/E force field³⁴. Our simulation cell contains 38 water molecules with periodic boundary conditions ($8\text{\AA} \times 8\text{\AA} \times 17.73\text{\AA}$), and the projectile proton travels in the +z direction. This simulation was compared to a larger simulation cell with 170 water molecules ($12\text{\AA} \times 12\text{\AA} \times 35.45\text{\AA}$), and no appreciable finite size errors were found. In order to determine electronic stopping power accurately using the non-equilibrium simulation approach, an ensemble average of projectile proton trajectories is necessary²³. 64 proton projectile trajectories (paths) were sampled evenly on a grid dividing the cross section of the xy simulation cell plane. In total, 64 independent RT-TDDFT

simulations were performed for each velocity. The convergence of this sampling was confirmed by comparing to a more extensive sampling that includes 256 paths. Albeit computationally expensive, this trajectory sampling ensures that the ensemble average contains projectile proton trajectories that cover a wide range of impact parameters with respect to the atoms in the target matter, which is especially important when core electrons are excited^{23,35}. The error bars on the stopping power reported here are the standard error of the mean calculated based on these 64 paths. Because the K-shell core electron excitation is found to be important in the high velocity regime, we also verified that close/small impact parameters are accurately sampled. These technical, but important, details are discussed in the Supplemental Material, in addition to comparisons to our earlier work¹⁸, which did not consider core electron effects.

The calculated stopping power as a function of the proton velocity ranging from 0.5 to 8 a.u. (corresponding to the kinetic energy of 6.2 keV-1.6 MeV) is compared to the available experimental stopping power data³⁶⁻³⁷ and to the so-called SRIM¹⁶ model in Figure 1. The only experimental data available in this velocity range are the measurements by Shimizu, et al.³⁶⁻³⁷. We note, for completeness, that the reliability of this measurement has been questioned on the basis of the Bethe model³⁸. The SRIM model is based on extending the Lindhard-Scharff-Schiott theory³⁹ with inputs from available experiments, and it is widely used as a standard reference. Though there is no reported experimental data for velocities less than 3.5 a.u. for liquid water, the SRIM result relies on existing experimental data of solid water (ice) to estimate the stopping power of liquid water. Our first-principles result is in excellent agreement with these two references. The peak of our calculated stopping power (i.e. the Bragg peak) is at $v=1.73$ a.u., and the stopping power of 0.165 ± 0.010 a.u. agrees well with the SRIM model which shows the Bragg peak at $v=1.72$ a.u. and stopping power of 0.165 a.u. at this velocity. For comparison, we also show the seminal Bethe model⁴⁰ with mean excitation energy parameter of $I=78\text{eV}$ as recommended by the International Commission on Radiation Units and Measurement⁸ and one of the most recent models by Emfietzoglou and co-workers¹⁰⁻¹² based on perturbation theory. For the Bethe model, the Bragg peak lies around $v=1.98$ a.u. with a corresponding stopping power of 0.160 a.u.. As widely recognized, the Bethe model significantly underestimates the stopping power for low projectile velocities, and it does not obey the correct linear dependence around zero velocity⁴¹. At the same time, the Bethe model is remarkable in that the model correctly captures the stopping power behavior for the large projectile velocities beyond the peak velocity with only a single parameter to account for the target

matter, the mean excitation energy. The Emfietzoglou's model goes beyond the Bethe model, and it tends to the correct limits in both low and high velocities. However, Emfietzoglou's model shows the Bragg peak at around $v=1.80$ a.u. with the stopping power of 0.130 a.u., which significantly underestimates the magnitude of the electronic stopping power with respect to our first-principles result.

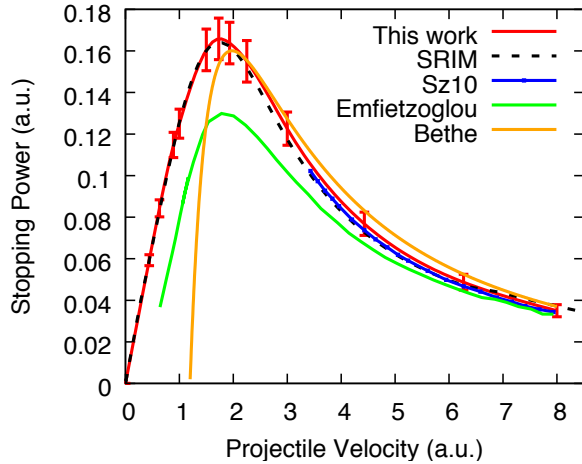


FIG 1 Electronic stopping power curve from our first-principles simulation, in comparison to the experimental data by Shimizu et al.³⁶⁻³⁷ (Sz10), SRIM¹⁶ model, the Bethe model⁴⁰ with $I=78$ eV recommended by International Commission on Radiation Units and Measurement⁸, and the Emfietzoglou's model¹⁰⁻¹².

One of the most pressing challenges is to elucidate the importance of the K-shell core electron excitations. Widely used in radiation oncology, X/ γ -ray radiation could effectively excite deep core electrons, undergoing Auger effect⁴². Empirical models have indicated that proton radiation does not excite K-shell core electrons appreciably for the proton velocities near the Bragg peak but only for much large velocities¹¹. In recent years, differences between X/ γ -ray and proton radiation have been examined more carefully in the radiation therapy literature¹⁹. However, our understanding of proton radiation is still quite limited, even for such an important biological matters like liquid water. Here, we examine the extent to which the K-shell core electron excitations play a role in the electronic stopping of protons in liquid water. In the literature, a separate K-shell contribution to stopping power is widely used, as in the Emfietzoglou's model¹². However, in addition to providing an extra channel for the energy transfer from the projectile proton, electronic excitations of K-shell core electrons also influence the valence electron excitations. This is commonly known as "shake-up" effect⁴³ in the related context of X-ray absorption. In reality, it is therefore not possible to separate the electronic stopping power in terms

of contributions from the valence electrons and core electrons independently as is widely done in empirical models^{11-12,44-47}. Using first-principles theory, we can quantify how much the stopping power is influenced by the presence of the K-shell core electrons by calculating the stopping power with and without including the core electrons in our simulations as shown in the top panel of Figure 2. For convenience, we refer to the difference in these two stopping power curves as ΔS^{core} . The valence electron contribution indeed accounts for >99% of the stopping power for velocities less than 1.5 a.u. However, for the velocities larger than 1.5 a.u., the K-shell stopping power contribution, ΔS^{core} , starts to increase, from 0.002 a.u. (2% of the stopping power) at $v=1.73$ a.u. to 0.012 a.u. (25% of the stopping power) at $v=6.27$ a.u.. For the highest velocity of 8.0 a.u. we considered here, the stopping power is 28% higher when the core electrons are present. This observation differs significantly from the estimated K-shell electron contribution based on various empirical models (Emfietzoglou/Drude¹¹⁻¹² and Hydrogenic generalized oscillator strength^{11, 45, 48-49}) as shown in the bottom panel of Figure 2. For instance, the Emfietzoglou's model¹² predicts that the K-shell contribution starts to become important only at much greater velocities of > 3.5 a.u. (Figure 2 (Bottom)), and K-shell core electrons are responsible for less than 10% of the stopping power even at $v=8.0$ a.u..

* E-mail: ykanai@unc.edu

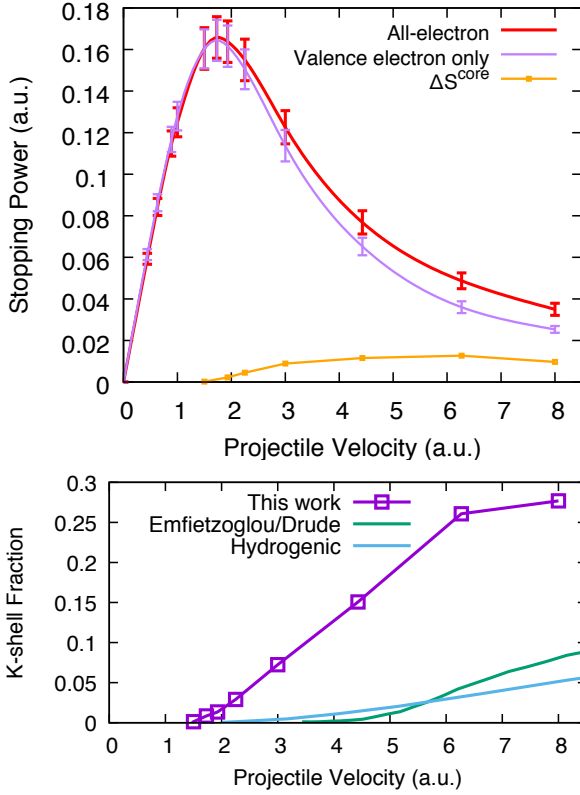


FIG 2 (Top) Contribution of the K-shell (oxygen 1s electrons) excitation to electronic stopping power curve, ΔS^{core} , calculated as the difference between the all-electron and the valence-electron only results. (Bottom) The fraction of the K-shell contribution to the stopping power, in comparison to the Emfietzoglou/Drude model¹¹⁻¹², and Hydrogenic generalized oscillator strength model^{11, 45, 48-49}.

As discussed above, K-shell core electron excitations not only provide an extra channel for the energy transfer, but they also influence valence electron excitations. To quantify this shake-up effect in the electronic stopping, we calculated the summed expectation value of the Kohn-Sham (KS) Hamiltonian for all the valence electron wavefunctions, $\sum \langle \varphi_i(t) | \hat{H}_{KS} | \varphi_i(t) \rangle$, in the simulations with and without the core electrons. The shake-up effect then can be quantified by obtaining the difference of this Hamiltonian expectation values for the valence electrons in the simulations with and without the K-shell core electrons. Figure 3 shows this energy difference as a function of the projectile proton displacement, averaged over all the 64 projectile paths. The shake-up effect contribution to the stopping power is obtained by calculating this expectation value change per unit distance of the projectile proton

movement. At the high proton velocity of 8.0 a.u., the shake-up effect is responsible for 36 % of ΔS^{core} (i.e. 11 % of the stopping power). At the Bragg peak proton velocity of 1.73 a.u., 56 % of ΔS^{core} is due to the shake-up effect, but it is only <1% of the stopping power because K-shell core electrons are hardly excited at this peak velocity. For a very low velocity of 1.00 a.u., no shake-up effect is observed, and the difference between the all-electron and valence-electron-only calculations simply oscillates around zero in Figure 3. The K-shell core electron excitations have significant influence on the valence electron excitations at high velocities. Although having a separate correction for the core electron excitation is convenient in modeling^{12, 23}, it is not possible to take into account this intricate shake-up effect using such a model correction. This shake-up effect partly explains why using a separate K-shell correction underestimates the ΔS^{core} with respect to our first-principles result (see Figure 2 (bottom)).

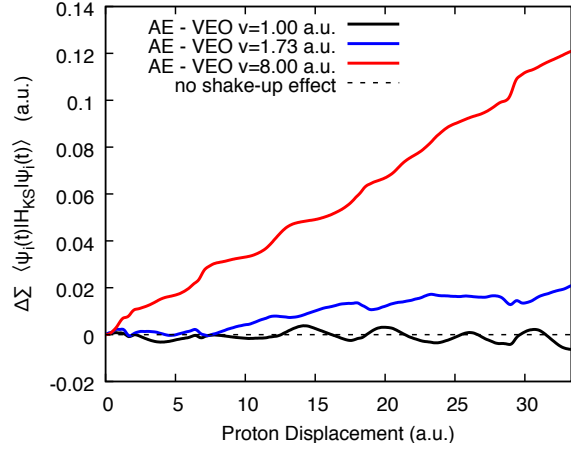


FIG 3 Difference of the summed Hamiltonian expectation value of the valence electrons for simulations with (all electrons - AE) and without K-shell core electrons (valence electron only - VEO) at the projectile proton velocity of 1.00 a.u., 1.73 (peak) and 8.00 a.u..

Having examined the K-shell core electron excitations and the importance of the shake-up effect, we now turn our attention to the spatial characteristics of the excited carriers in the electronic stopping process. The time-dependent Kohn-Sham (KS) wavefunctions can be projected onto the KS eigenstates of the equilibrium electrons to obtain the excited carrier distribution¹⁷⁻¹⁸. The projection onto the occupied and unoccupied eigenstates is used to calculate the hole and excited electron populations, respectively. All the occupied eigenstates and the unoccupied eigenstates up to 80 eV above the conduction band minimum are included in the projection, and the

electronic states covered in this energy range account for greater than 95% of the total excited electrons. At the peak velocity of $v=1.73$ a.u., the average number of holes per water molecule is 0.0933, and only 0.003% (3×10^{-6} holes) are generated in the K-shell. At $v=8.0$ a.u., the average number of holes is significantly smaller, 0.0108, but approximately 1% (1×10^{-4} holes) of the holes are generated in the K-shell. Figure 4 shows the spatial distribution of the excited electrons and holes at $v=8.0$ a.u., as a function of the distance from each projectile proton path, averaged over all the projectile paths. A full width at half maximum (FWHM) of the distribution for the core holes is 0.40 Å, while a noticeably broader FWHM of 2.38 Å is observed for the hole distribution in the valence band states. The valence hole distribution shows two notable features: a localized region that corresponds to individual water molecules along the path and the distribution tail that derives from neighboring water molecules. This tail component gives the valence hole distribution an appreciable magnitude even at distances larger than 5 Å. On the other hand, the excited electron distribution is not so localized along the projectile proton path as shown in Figure 4, and the excited electron distribution decreases only by $\sim 10\%$ even at 5 Å away from the path. This indicates that individual water molecules are indeed ionized along the projectile path in the electronic stopping process, consistent with our earlier finding¹⁷ and also with the established notion of proton radiation as ionizing radiation. The K-shell core electron excitations still contribute greatly to the stopping power even when only a small proportion of the excited electrons are excited from the K-shell core states because the core excitation energy is a few orders of magnitude greater than the valence excitation energy.

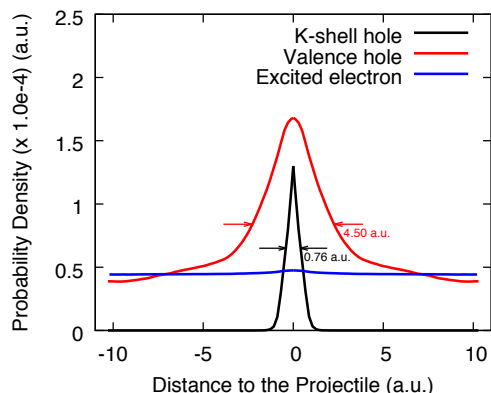


FIG 4 Ensemble-averaged distribution of holes and excited electrons as a function of the distance from the projectile proton path at the proton velocity of 8.0 a.u., the plot is made symmetric as a guide to the eye. The arrows indicate the FWHMs of the valence hole and O 1s hole distributions.

Developing a detailed understanding of the role of core electron excitations in liquid water under proton irradiation has become important largely due to the growing use of proton beams in radiation oncology. Using non-equilibrium simulations based on real-time time-dependent density functional theory, we accurately determined the electronic stopping power for protons in water from first principles, particularly focusing on the role of core electrons. The first-principles predicted stopping power shows significant differences to commonly-used perturbation theoretic models, such as the Bethe and Emfietzoglou models^{12-13, 40}. The K-shell core electron excitation from water molecules' oxygen atoms was found to be crucial in determining the electronic stopping power curve beyond its maximum, being responsible for as much as one-third of the stopping power at the large proton velocity of 8.0 a.u. (the kinetic energy of 1.6 MeV). The core electron excitation significantly influences the valence electron excitation, in addition to providing an additional channel for the energy transfer. Such a cooperative phenomenon in the excitation is often referred to as the shake-up effect⁴³, and this effect approximately accounts for as much as half of the contribution of the K-shell core electron excitation to the electronic stopping power at the high proton velocity of 8.0 a.u.. In the excitation process, the generated holes remain highly localized within a few angstroms around the irradiating proton path while electrons are excited away, indicative of ionizing radiation behavior. Despite their importance in contributing to the stopping power, the K-shell core electrons play a rather minor role in terms of the excitation density; only 1% of the holes is generated in the K-shell even at the large velocity of 8.0 a.u.. While X/ γ -ray and proton radiations are both considered to be ionizing radiation and are usually treated on the same footing¹⁹, our work revealed that the excitation/ionization behaviors involved are distinctly different.

ACKNOWLEDGMENTS

The work is supported by the National Science Foundation under Grants No. CHE-1565714, No. DGE-1144081, and No. OAC-1740204. An award of computer time was provided by the Innovative and Novel Computational Impact on Theory and Experiment (INCITE) program. This research used resources of the Argonne Leadership Computing Facility, which is a DOE Office of Science User Facility supported under Contract DE-AC02-06CH11357.

REFERENCE

1. Race, C. P.; Mason, D. R.; Finnis, M. W.; Foulkes, W. M. C.; Horsfield, A. P.; Sutton, A. P., The treatment of electronic excitations in atomistic models of radiation damage in metals. *Reports on Progress in Physics* **2010**, 73 (11), 116501.

* E-mail: ykanai@unc.edu

2. Ziegler, J. F., Stopping of energetic light ions in elemental matter. *Journal of Applied Physics* **1999**, *85* (3), 1249-1272.
3. Scholz, M., Heavy ion tumour therapy. *Nucl Instrum Meth B* **2000**, *161*, 76-82.
4. Stelzer, H., Tumor therapy with heavy ions at GSI. *Nucl Phys B* **1998**, 650-657.
5. Kamaratos, E., The Mean Excitation-Energy for Stopping Power-I, the Bragg Rule, and Chemical and Phase Effects - Application of a Statistical Treatment to the Determination of I for Chemically Bound Particles. *Chem Rev* **1984**, *84* (6), 561-576.
6. Sigmund, P., *PARTICLE PENETRATION AND RADIATION EFFECTS: General Aspects and Stopping of Swift Point Charges* Springer: 2006; Vol. 151.
7. Sabin, J. R.; Oddershede, J.; Cabrera-Trujillo, R.; Sauer, S. P. A.; Deumens, E.; Öhrn, Y., Stopping power of molecules for fast ions. *Molecular Physics* **2010**, *108* (21-23), 2891-2897.
8. Report 90. *Journal of the International Commission on Radiation Units and Measurements* **2014**, *14* (1), 34-37.
9. Ashley, J. C., Optical-data model for the stopping power of condensed matter for protons and antiprotons. *Journal of Physics: Condensed Matter* **1991**, *3* (16), 2741.
10. Emfietzoglou, D.; Cucinotta, F. A.; Nikjoo, H., A Complete Dielectric Response Model for Liquid Water: A Solution of the Bethe Ridge Problem. *Radiation Research* **2005**, *164* (2), 202-211.
11. Emfietzoglou, D.; Garcia-Molina, R.; Kyriakou, I.; Abril, I.; Nikjoo, H., A dielectric response study of the electronic stopping power of liquid water for energetic protons and a new I-value for water. *Physics in Medicine & Biology* **2009**, *54* (11), 3451.
12. Emfietzoglou, D.; Nikjoo, H.; Pathak, A., Electronic cross sections for proton transport in liquid water based on optical-data models. *Nuclear Instruments and Methods in Physics Research Section B: Beam Interactions with Materials and Atoms* **2006**, *249* (1), 26-28.
13. Garcia-Molina, R.; Abril, I.; de Vera, P.; Kyriakou, I.; Emfietzoglou, D., A study of the energy deposition profile of proton beams in materials of hadron therapeutic interest. *Applied Radiation and Isotopes* **2014**, *83*, 109-114.
14. Penn, D. R., Electron mean-free-path calculations using a model dielectric function. *Physical Review B* **1987**, *35* (2), 482-486.
15. Ritchie, R. H., Energy losses by swift charged particles in the bulk and at the surface of condensed matter. *Nuclear Instruments and Methods in Physics Research* **1982**, *198* (1), 81-91.
16. Ziegler, J. F.; Ziegler, M. D.; Biersack, J. P., SRIM – The stopping and range of ions in matter (2010). *Nuclear Instruments and Methods in Physics Research Section B: Beam Interactions with Materials and Atoms* **2010**, *268* (11), 1818-1823.
17. Reeves, K. G.; Kanai, Y., Electronic Excitation Dynamics in Liquid Water under Proton Irradiation. *Scientific Reports* **2017**, *7*, 40379.
18. Reeves, K. G.; Yao, Y.; Kanai, Y., Electronic stopping power in liquid water for protons and alpha particles from first principles. *Physical Review B* **2016**, *94* (4), 041108.
19. Durante, M.; Orecchia, R.; Loeffler, J. S., Charged-particle therapy in cancer: clinical uses and future perspectives. *Nature Reviews Clinical Oncology* **2017**, *14*, 483.
20. Schleife, A.; Draeger, E. W.; Kanai, Y.; Correa, A. A., Plane-wave pseudopotential implementation of explicit integrators for time-dependent Kohn-Sham equations in large-scale simulations. *The Journal of Chemical Physics* **2012**, *137* (22), 22A546.
21. Schleife, A.; Kanai, Y.; Correa, A. A., Accurate atomistic first-principles calculations of electronic stopping. *Physical Review B* **2015**, *91* (1), 014306.
22. Yost, D. C.; Kanai, Y., Electronic stopping for protons and alpha particles from first-principles electron dynamics: The case of silicon carbide. *Physical Review B* **2016**, *94* (11), 115107.
23. Yost, D. C.; Yao, Y.; Kanai, Y., Examining real-time time-dependent density functional theory nonequilibrium simulations for the calculation of electronic stopping power. *Physical Review B* **2017**, *96* (11), 115134.
24. Pruneda, J. M.; Sánchez-Portal, D.; Arnau, A.; Juaristi, J. I.; Artacho, E., Electronic Stopping Power in LiF from First Principles. *Physical Review Letters* **2007**, *99* (23), 235501.
25. Schleife, A.; Draeger, E. W.; Anisimov, V. M.; Correa, A. A.; Kanai, Y., Quantum Dynamics Simulation of Electrons in Materials on High-Performance Computers. *Computing in Science & Engineering* **2014**, *16* (5), 54-60.
26. Gygi, F., Qbox open source code project. *Tech. Rep. (University of California, Davis)*.
27. Gygi, E. W. D. a. F., Qbox code, Qb@ll version. *Tech Rep. (Lawrence Livermore National Laboratory)*.
28. Hamann, D. R., Optimized norm-conserving Vanderbilt pseudopotentials. *Physical Review B* **2013**, *88* (8), 085117.
29. Schlipf, M.; Gygi, F., Optimization algorithm for the generation of ONCV pseudopotentials. *Computer Physics Communications* **2015**, *196*, 36-44.
30. Perdew, J. P.; Burke, K.; Ernzerhof, M., Generalized Gradient Approximation Made Simple. *Physical Review Letters* **1996**, *77* (18), 3865-3868.
31. Sun, J.; Remsing, R. C.; Zhang, Y.; Sun, Z.; Ruzsinszky, A.; Peng, H.; Yang, Z.; Paul, A.; Waghmare, U.; Wu, X.; Klein, M. L.; Perdew, J. P., Accurate first-principles structures and energies of diversely bonded systems from an efficient density functional. *Nature Chemistry* **2016**, *8*, 831.
32. Sun, J.; Ruzsinszky, A.; Perdew, J. P., Strongly Constrained and Appropriately Normed Semilocal Density Functional. *Physical Review Letters* **2015**, *115* (3), 036402.
33. Yao, Y.; Kanai, Y., Plane-wave pseudopotential implementation and performance of SCAN meta-GGA exchange-correlation functional for extended systems. *The Journal of Chemical Physics* **2017**, *146* (22), 224105.
34. Berendsen, H. J. C.; Grigera, J. R.; Straatsma, T. P., The missing term in effective pair potentials. *The Journal of Physical Chemistry* **1987**, *91* (24), 6269-6271.
35. Ullah, R.; Artacho, E.; Correa, A. A., Core Electrons in the Electronic Stopping of Heavy Ions. *Physical Review Letters* **2018**, *121* (11), 116401.
36. Shimizu, M.; Hayakawa, T.; Kaneda, M.; Tsuchida, H.; Itoh, A., Stopping cross-sections of liquid water for 0.3–2.0 MeV protons. *Vacuum* **2010**, *84* (8), 1002-1004.

37. Shimizu, M.; Kaneda, M.; Hayakawa, T.; Tsuchida, H.; Itoh, A., Stopping cross sections of liquid water for MeV energy protons. *Nuclear Instruments and Methods in Physics Research Section B: Beam Interactions with Materials and Atoms* **2009**, 267 (16), 2667-2670.
38. Garcia-Molina, R.; Abril, I.; de Vera, P.; Paul, H., Comments on recent measurements of the stopping power of liquid water. *Nuclear Instruments and Methods in Physics Research Section B: Beam Interactions with Materials and Atoms* **2013**, 299, 51-53.
39. Lindhard, J.; Nielsen, V.; Scharff, M.; Thomsen, P., Integral equations governing radiation effects. *Mat. Fys. Medd. Dan. Vid. Selsk* **1963**, 33 (10), 1-42.
40. Bethe, H., Zur theorie des durchgangs schneller korpussularstrahlen durch materie. *Annalen der Physik* **1930**, 397 (3), 325-400.
41. Ahlen, S. P., Theoretical and experimental aspects of the energy loss of relativistic heavily ionizing particles. *Reviews of Modern Physics* **1980**, 52 (1), 121-173.
42. Yokoya, A.; Ito, T., Photon-induced Auger effect in biological systems: A review. *International journal of radiation biology* **2017**, 93 (8), 743-756.
43. Persson, P.; Lunell, S.; Szöke, A.; Ziaja, B.; Hajdu, J., Shake-up and shake-off excitations with associated electron losses in X-ray studies of proteins. *Protein Science* **2001**, 10 (12), 2480-2484.
44. Garcia-Molina, R.; Abril, I.; Heredia-Avalos, S.; Kyriakou, I.; Emfietzoglou, D., A combined molecular dynamics and Monte Carlo simulation of the spatial distribution of energy deposition by proton beams in liquid water. *Physics in Medicine & Biology* **2011**, 56 (19), 6475.
45. Dingfelder, M.; Inokuti, M.; Paretzke, H. G., Inelastic-collision cross sections of liquid water for interactions of energetic protons. *Radiation physics and chemistry* **2000**, 59 (3), 255-275.
46. Date, H.; Sutherland, K.; Hayashi, T.; Matsuzaki, Y.; Kiyonagi, Y., Inelastic collision processes of low-energy protons in liquid water. *Radiation Physics and Chemistry* **2006**, 75 (2), 179-187.
47. Bernal, M.; Liendo, J., Inelastic-collision cross sections for the interactions of totally stripped H, He and C ions with liquid water. *Nuclear Instruments and Methods in Physics Research Section B: Beam Interactions with Materials and Atoms* **2007**, 262 (1), 1-6.
48. Heredia-Avalos, S.; Garcia-Molina, R.; Fernández-Varea, J. M.; Abril, I., Calculated energy loss of swift He, Li, B, and N ions in Si O 2, Al 2 O 3, and Zr O 2. *Physical Review A* **2005**, 72 (5), 052902.
49. Garcia-Molina, R.; Abril, I.; Denton, C. D.; Heredia-Avalos, S.; Kyriakou, I.; Emfietzoglou, D., Calculated depth-dose distributions for H⁺ and He⁺ beams in liquid water. *Nuclear Instruments and Methods in Physics Research Section B: Beam Interactions with Materials and Atoms* **2009**, 267 (16), 2647-2652.
50. See Supplemental Material [url] for computational details and comparison to earlier RT-TDDFT result and empirical/analytical models, which includes refs. [51-53].
51. Nilsson, A.; Nordlund, D.; Waluyo, I.; Huang, N.; Ogasawara, H.; Kaya, S.; Bergmann, U.; Näslund, L. Å.; Öström, H.; Wernet, P.; Andersson, K. J.; Schiros, T.; Pettersson, L. G. M., X-ray absorption spectroscopy and X-ray Raman scattering of water and ice; an experimental view. *Journal of Electron Spectroscopy and Related Phenomena* **2010**, 177 (2), 99-129.
52. Fonseca Guerra, C.; Handgraaf, J. W.; Baerends, E. J.; Bickelhaupt, F. M., Voronoi deformation density (VDD) charges: Assessment of the Mulliken, Bader, Hirshfeld, Weinhold, and VDD methods for charge analysis. *Journal of computational chemistry* **2004**, 25 (2), 189-210.
53. Schiwietz, G.; Grande, P., Improved charge-state formulas. *Nuclear Instruments and Methods in Physics Research Section B: Beam Interactions with Materials and Atoms* **2001**, 175, 125-131.

* E-mail: ykanai@unc.edu

Supplemental Material for

“K-shell Core Electron Excitation in Electronic Stopping of Protons in Water from First Principles”

Yi Yao, Dillon C. Yost, and Yosuke Kanai

Department of Chemistry, University of North Carolina at Chapel Hill

Computational Details

Planewave expansion and projectile proton

An important aspect of the accurate calculation of liquid water electronic stopping power for large velocities is the treatment of the proton projectile as a bare Coulomb potential. The bare Coulomb potential is significantly different than the pseudopotential, especially in the core region, leading to differences in electronic stopping power for large velocities. In Figure S1, the real-time time-dependent density functional theory (RT-TDDFT)-calculated stopping power data for $v=8.0$ a.u. is shown. When only valence electrons are explicitly treated using pseudopotentials for liquid water atoms and a pseudopotential is used also for the projectile proton, the electronic stopping power is 0.025 a.u.. When *all the electrons* are explicitly treated using pseudopotentials for liquid water atoms and a pseudopotential is used also for the projectile proton, the electronic stopping power is 0.028 a.u.. For this case, a very large planewave energy cutoff of 200 Ry is required to achieve the convergence. If *all the electrons* are explicitly treated using pseudopotentials for liquid water atoms and the projectile proton is represented exactly by using the bare Coulomb potential, the calculated stopping power is 0.035 a.u.. With the bare Coulomb potential proton projectile, the K-shell contribution to the stopping power is 3.5 times higher than the K-shell contribution calculated with the pseudopotential proton projectile.

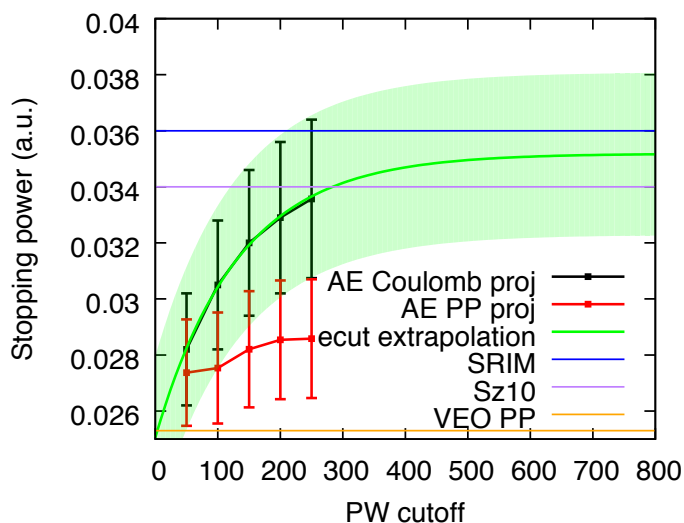


Figure S1: Convergence of the stopping power at the velocity of 8.0 a.u. AE Coulomb proj. (black) – All-electron calculation with bare Coulomb potential for the proton projectile, AE PP proj (red)– All-electron calculation with pseudopotential for the proton projectile, VEO PP proj (yellow) - Valence-electron only calculation with pseudopotential for the proton projectile. The planewave cutoff extrapolation (green) was performed with the formula of $A \cdot \exp(-B) + C$.

By projecting the time-dependent Kohn-Sham (TDKS) wavefunctions onto the ground state KS eigenfunctions, we acquire hole and excited electron distributions. As shown in Figure S2, with a proton projectile approximated by the pseudopotential, the hole population density of the K-shell is a small and smooth distribution. However, with the proton projectile represented by the Coulomb potential, the hole population for the K-shell is much larger and sharper.

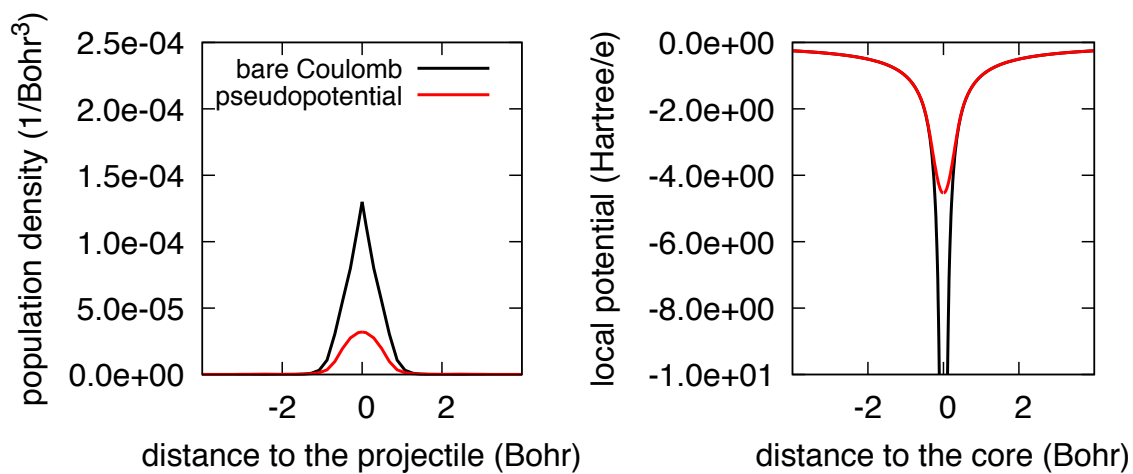


Figure S2: (Left) Population distribution for Oxygen 1s hole generated by bare the Coulomb proton projectile and the pseudopotential proton projectile. (Right) The local part of the pseudopotentials and bare Coulomb potential used for the projectile proton are shown.

Projectile Proton Path Ensemble

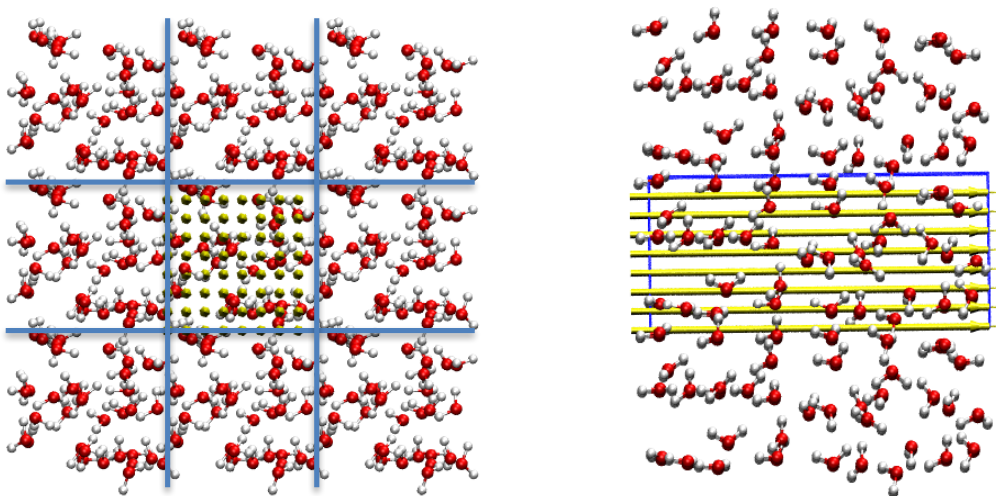


Figure S3. Front (left panel) and side (right panel) views of the sampled projectile paths for the stopping power calculations. The blue lines indicate the boundaries of the simulation cell that is periodically repeated.

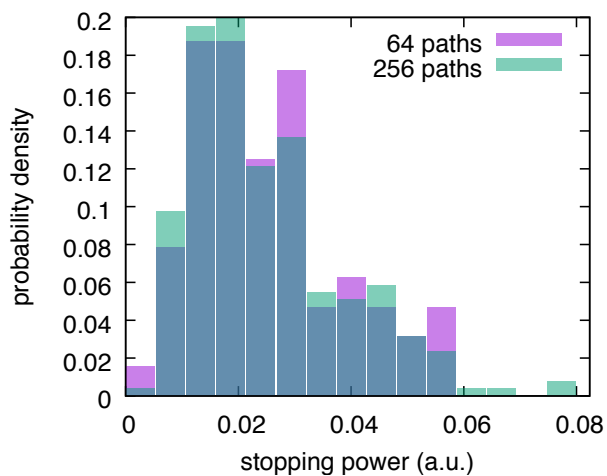


Figure S4. Path-dependent stopping power distribution for a proton with a velocity of 8.0 a.u. for the 64-paths ensemble (purple), compared to a 256-path ensemble (green). Valence-electron only calculations with a pseudopotential for the proton projectile were used.

Impact Parameter Sampling

Because the oxygen K-shell core electron excitation was found to be significant, having an accurate sampling of close (i.e. small) impact parameters is particularly important in the high velocity regime (e.g. $v \approx 8$ a.u.). For the electronic stopping power calculation, a classical ensemble average is taken over the 64 projectile (discussed above) proton trajectories in which the projectile proton is constrained to move along a straight path. In order to verify that deflection of the projectile proton by water molecules is negligible, Ehrenfest dynamics, using the RT-TDDFT forces, was performed for $v=8$ a.u.. Figure S5 shows how much the closest impact parameter changes for each of the 64 trajectories. As can be seen, whether we use the constrained or Ehrenfest dynamics, the trajectories are negligibly influenced in the sampling for even very small impact parameters. Because the average velocity remains close to $v=8$ a.u. at the end of the Ehrenfest dynamics ($v=7.99992$ a.u., to be specific), it is reasonable to calculate the stopping power for the Ehrenfest trajectories. This yields the stopping power value of $0.034979 (\pm 0.002944)$ a.u., which is essentially identical to the stopping power of $0.034999 (\pm 0.002943)$ for $v=8$ a.u., further validation that using the constrained trajectories has no effect on the impact parameter sampling and the stopping power calculation.

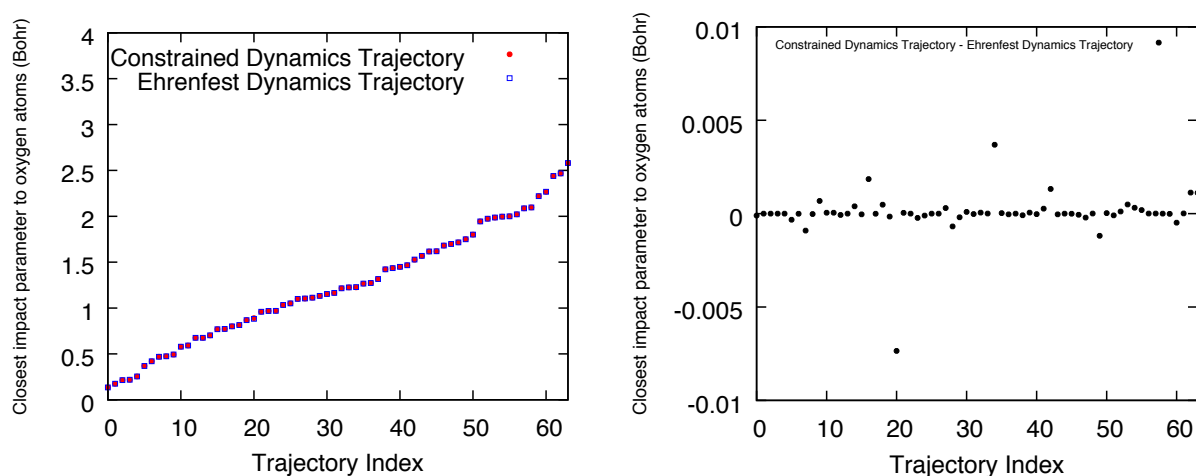


Figure S5. The closest impact parameter to oxygen atoms for all 64 trajectories. The trajectory indices are ordered by the closest impact parameter. (left) Absolute values for the Constrained Dynamics Trajectory and Ehrenfest Dynamics Trajectory. (right) The difference between Constrained Dynamics Trajectory and Ehrenfest Dynamics Trajectory.

Simulation Cell Size

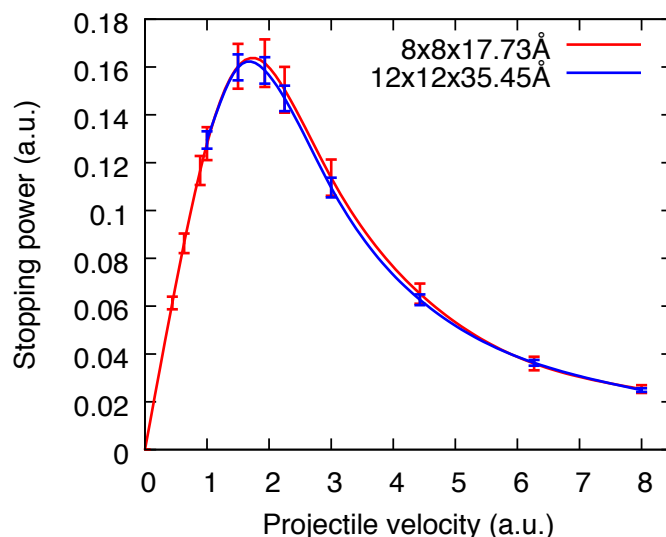


Figure S6. The stopping power curve calculated using simulation cell sizes of $8 \times 8 \times 17.73 \text{ \AA}$ and of $12 \times 12 \times 35.45 \text{ \AA}$ with periodic boundary conditions. Valence-electron only simulations with a pseudopotential for the proton projectile were used.

Exchange Correlation (XC) Approximation Dependence: PBE GGA vs. SCAN meta-GGA

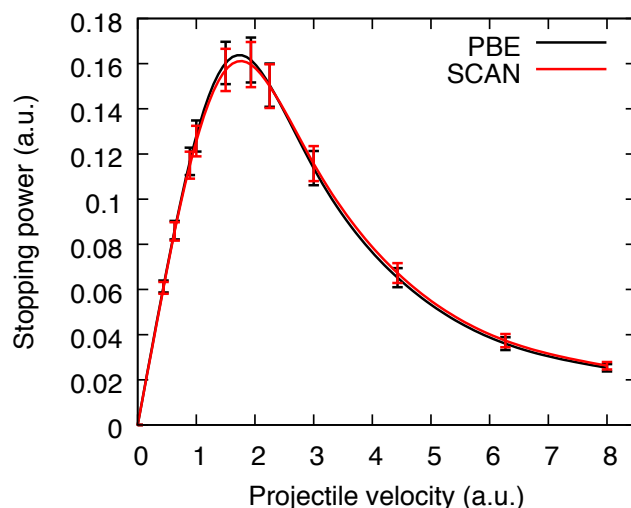


Figure S7: The stopping power curves calculated using the SCAN meta-GGA XC approximation and PBE GGA XC approximation. Valence-electron only simulations with a pseudopotential for the proton projectile were used.

Optical Excitation from 1s K-Shell in A Water Molecule

Because the plane-wave pseudopotential (PW-PP) formalism is generally not used for describing core electrons, we assessed the level of accuracy it can provide for modeling 1s K-shell optical excitation. The multi-projector approach by Hamann¹, enabled us to include the 1s electron in the calculation, as discussed in the main text. Using a RT-TDDFT simulation with the all-electron (AE) pseudopotential formalism, one is able to model the K-edge excitation from 1s electron of oxygen atoms in a water molecule while the valence-electron only (VEO) pseudopotential expectedly does not show the corresponding optical excitation. The K-edge of the absorption spectrum is in good agreement with the experimental measurement.

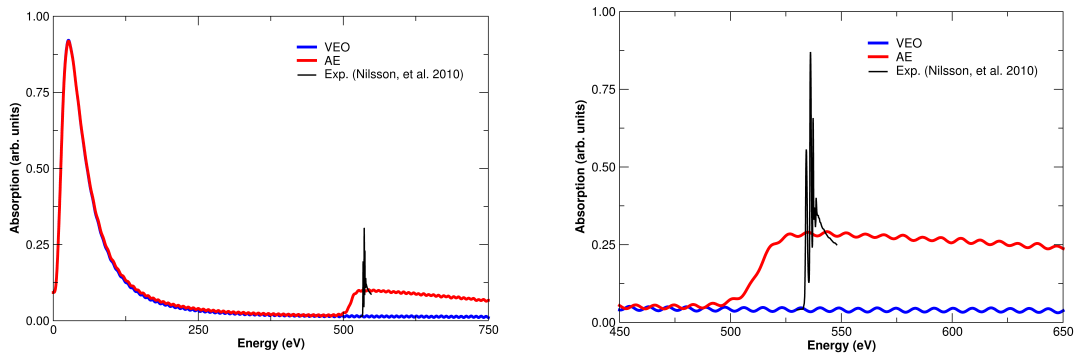


Figure S8. Single water molecule RT-TDDFT absorption spectra for the valence electron only (blue) and all-electron (red) cases. The all-electron RT-TDDFT K-shell core excitation onset is compared to the experimental X-ray absorption peak (black)².

Excitation Density

Supplement to Figure 4 (in main text) including plots for the proton velocity of 1.73 a.u. (left panels) at the Bragg peak. Additionally, logarithmic scale plots are shown (bottom panels), as is necessary for the $v=1.73$ a.u. case because of the extremely small contribution to the hole density from the 1s K-shell of the oxygen atoms in water molecules.

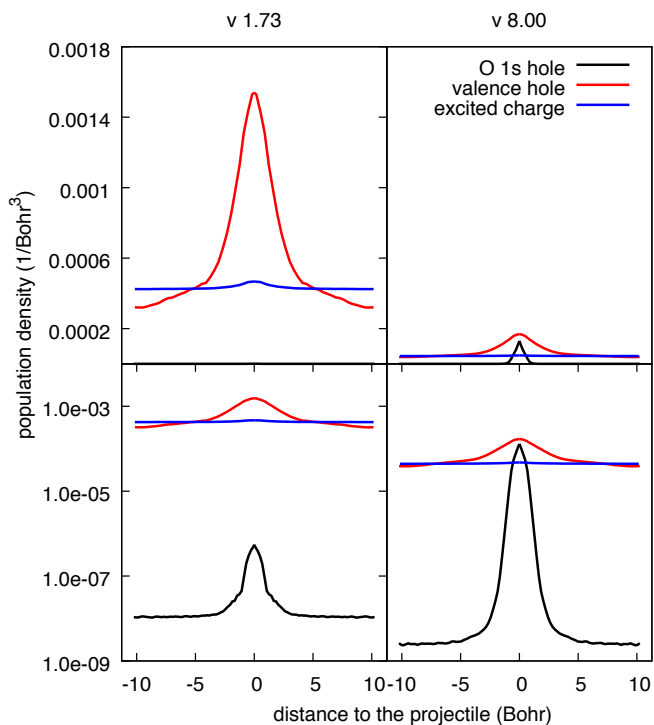


Figure S9. Ensemble-averaged distribution of holes and excited electrons as a function of the distance to the projectile proton path for the velocities of 1.73 (Bragg Peak) and 8.0 a.u., for convenience, the plot has been made symmetric. The logarithmic scale plots in the bottom reveal the small contribution to the total hole population from the oxygen 1s K-shell.

Charge State of Projectile Proton

We calculated the charge state of the projectile ion from a summation of the electron density in its Voronoi cell³. The equilibrium electron density is first subtracted from the velocity-dependent, non-equilibrium electron density so that the electron density of liquid water does not contribute to the projectile ion charge⁴.

We extract the charge state information from our first-principles calculation. The Schiwietz and Grande model⁵ is also plotted for comparison. Note that the charge state is not an input for the RT-TDDFT simulations. Rather, it is a quantity that can be extracted from the induced electron density after the charge has reached a steady state on the projectile ion.

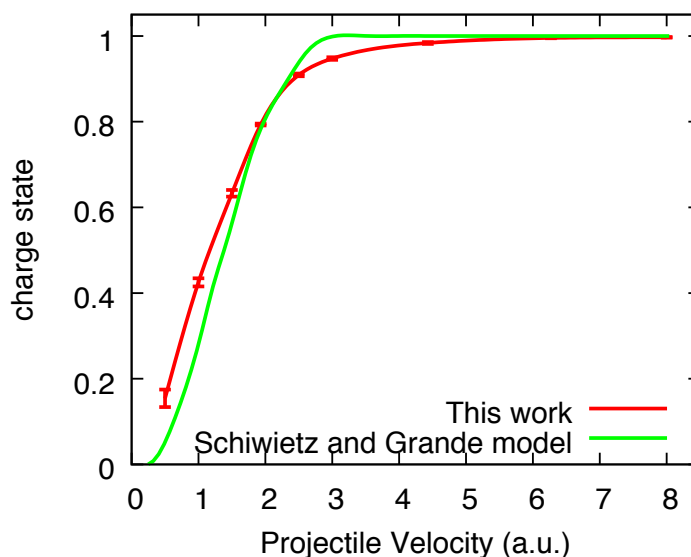


Figure S10. Mean steady-state charge for a proton projectile in liquid water as a function of the projectile ion velocity. Error bars represent the standard deviations of the distribution of the instantaneous charge state, which is calculated using the Voronoi partitioning³ in the simulation. The empirical model for the projectile charge state by Schiwietz and Grande⁵ is shown as green line for comparison.

Comparison to earlier RT-TDDFT result and empirical/analytical models

We compare the electronic stopping power curve obtained using RT-TDDFT to our earlier work (Reeves, et al)⁴ as well as to empirical/analytical models of Garcia-Molina⁶, Penn⁷⁻⁸, Ritchie⁸⁻⁹, Ashley^{8,10}, and Emfietzoglou⁸ discussed in our earlier work⁴. The work by Emfietzoglou, et al.⁸ gives a detailed discussion of the models by Penn, Ritchie, and Ashley, along with the parameters used. The difference (within the statistical bars) between this first-principles work and our earlier first-principles work⁴ derives from the inclusion of core electrons in our present work and also, to some extent, the more limited samplings of projectile proton paths in our earlier work⁴.

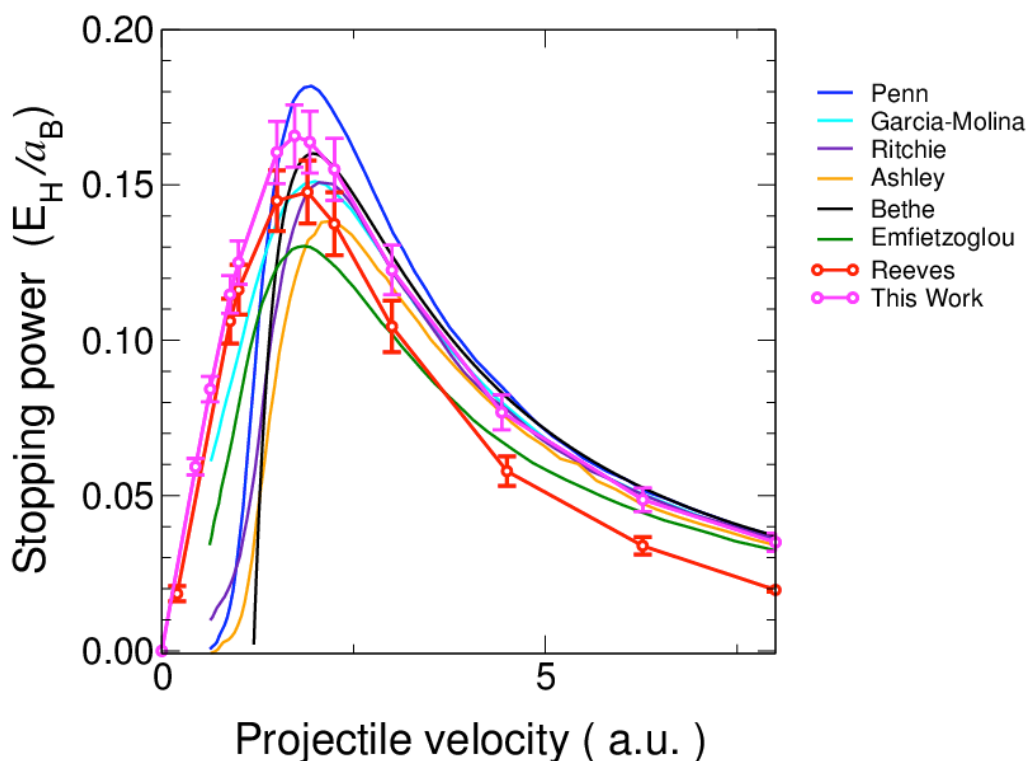


Figure S11. Electronic stopping power compared with our former work by Reeves, et al.⁴ (red) and analytical models using various model dielectric functions by Garcia-Molina⁶ (teal), Penn⁷⁻⁸ (blue), Ritchie⁸⁻⁹ (purple), Ashley^{8,10} (orange), and Emfietzoglou⁸ (green). The Bethe formula result (black) using a mean excitation energy of $I=78$ eV (the value currently recommended by the International Commission on Radiation Units and Measurement¹¹) is also plotted.

Liquid water structure

Cell vector a : 15.1178150222 0.0 0.0

Cell vector b : 0.0 15.1178150222 0.0

Cell vector c : 0.0 0.0 33.4969206901

atom	O1	O_species	11.2061	0.7370	24.1507
atom	H2	H_species	12.3210	1.3228	22.7523
atom	H3	H_species	10.6392	-1.0393	23.8106
atom	O4	O_species	5.5180	9.2030	6.7841
atom	H5	H_species	4.1763	8.3337	5.7826
atom	H6	H_species	4.7432	10.5069	7.9180
atom	O7	O_species	11.5651	2.4944	0.9827
atom	H8	H_species	13.1714	2.7590	0.0000
atom	H9	H_species	10.0911	2.8913	-0.1134
atom	O10	O_species	1.0016	3.8361	7.5400
atom	H11	H_species	0.7370	4.8188	5.9526
atom	H12	H_species	1.4929	5.0267	8.9384
atom	O13	O_species	13.1903	11.6974	18.2926
atom	H14	H_species	13.6249	12.0754	16.4973
atom	H15	H_species	12.3021	13.1903	19.0484
atom	O16	O_species	2.4377	14.2296	6.5951
atom	H17	H_species	2.1732	16.0816	6.6896
atom	H18	H_species	3.4204	13.8139	5.0456
atom	O19	O_species	10.6392	6.7463	15.5713
atom	H20	H_species	8.9573	7.4266	15.0422
atom	H21	H_species	11.7352	8.1825	16.1194
atom	O22	O_species	8.6361	1.7008	17.8957
atom	H23	H_species	8.5605	3.0614	19.2185
atom	H24	H_species	9.2975	2.4377	16.2705
atom	O25	O_species	3.6094	8.3526	22.8090
atom	H26	H_species	1.9275	7.5211	22.5633
atom	H27	H_species	4.7054	7.9935	21.3161
atom	O28	O_species	14.1541	11.6029	30.5569
atom	H29	H_species	15.7981	12.2454	29.8577
atom	H30	H_species	14.1541	11.8108	32.4466
atom	O31	O_species	0.7748	8.9384	9.5242
atom	H32	H_species	-0.6236	9.0140	8.2392
atom	H33	H_species	0.5102	10.3179	10.8092
atom	O34	O_species	8.7305	6.0471	21.2972
atom	H35	H_species	7.4077	6.7652	20.1634
atom	H36	H_species	7.8991	5.1212	22.7334

atom O37	O_species	6.5574	2.0031	3.5338
atom H38	H_species	6.3495	2.3622	1.6819
atom H39	H_species	8.3715	2.0976	3.9873
atom O40	O_species	6.7463	2.9102	31.7852
atom H41	H_species	7.5589	4.1196	30.5758
atom H42	H_species	6.3306	1.3039	30.8970
atom O43	O_species	10.8281	10.6959	23.8106
atom H44	H_species	11.3573	9.5998	25.2656
atom H45	H_species	10.7714	9.6376	22.2421
atom O46	O_species	4.2330	14.1163	17.9146
atom H47	H_species	5.9148	14.9288	18.2737
atom H48	H_species	3.5905	14.7210	16.2517
atom O49	O_species	6.1227	9.2030	0.8504
atom H50	H_species	5.4424	9.0707	-0.9071
atom H51	H_species	4.6865	9.1652	2.0787
atom O52	O_species	11.5840	1.5496	6.5385
atom H53	H_species	11.6596	1.7008	4.6487
atom H54	H_species	13.3226	1.7763	7.2566
atom O55	O_species	11.4328	7.0487	29.3853
atom H56	H_species	12.6045	8.4282	29.9522
atom H57	H_species	9.6754	7.7290	29.2719
atom O58	O_species	1.6819	14.6643	0.8693
atom H59	H_species	3.3448	15.2123	1.5874
atom H60	H_species	1.8519	14.4564	-1.0016
atom O61	O_species	6.4440	8.0880	27.8924
atom H62	H_species	6.6329	9.5809	26.7396
atom H63	H_species	5.5936	6.6896	26.9475
atom O64	O_species	11.1305	11.9242	11.9242
atom H65	H_species	11.6029	11.1872	10.2423
atom H66	H_species	10.2990	13.5871	11.6596
atom O67	O_species	0.7748	4.0251	12.8312
atom H68	H_species	0.5480	5.8959	12.8690
atom H69	H_species	-0.6614	3.2314	11.8864
atom O70	O_species	3.9117	13.2092	29.0262
atom H71	H_species	3.7984	13.0769	27.1554
atom H72	H_species	5.6881	12.8312	29.5931
atom O73	O_species	14.0974	7.1810	20.6925
atom H74	H_species	12.3777	6.4062	20.6169
atom H75	H_species	14.0218	8.9573	20.0500
atom O76	O_species	6.5196	8.3148	12.1887
atom H77	H_species	7.9935	9.5242	12.1698
atom H78	H_species	5.9148	8.0313	10.4313
atom O79	O_species	10.2990	2.3433	12.3399
atom H80	H_species	10.2234	4.0629	13.1147
atom H81	H_species	9.5053	2.4000	10.6203
atom O82	O_species	14.6643	1.6252	20.7114

atom	H83	H_species	15.2879	3.4015	20.7681
atom	H84	H_species	15.8737	0.5480	19.7287
atom	O85	O_species	1.1338	9.0140	3.7984
atom	H86	H_species	0.5480	7.9935	2.3244
atom	H87	H_species	0.2457	10.6770	3.8172
atom	O88	O_species	5.0078	6.8597	17.6689
atom	H89	H_species	3.8172	5.4046	17.7634
atom	H90	H_species	4.8566	7.6534	15.9493
atom	O91	O_species	9.1652	13.2470	28.6861
atom	H92	H_species	10.8281	13.1714	29.5931
atom	H93	H_species	9.4108	12.7179	26.8908
atom	O94	O_species	2.4755	14.2674	12.4344
atom	H95	H_species	3.4582	14.1541	10.8281
atom	H96	H_species	1.4929	15.8737	12.4722
atom	O97	O_species	13.5304	2.1543	29.0829
atom	H98	H_species	12.9068	3.9306	29.1585
atom	H99	H_species	13.2281	1.4362	27.3632
atom	O100	O_species	3.9306	13.7005	23.3759
atom	H101	H_species	3.5527	11.8864	23.0547
atom	H102	H_species	3.3259	14.7399	21.9208
atom	O103	O_species	11.2061	11.1305	1.6630
atom	H104	H_species	9.4297	10.6392	1.2472
atom	H105	H_species	11.2061	12.2265	3.2125
atom	O106	O_species	1.7385	6.2739	32.2387
atom	H107	H_species	1.6252	5.4802	30.5191
atom	H108	H_species	3.1936	5.5180	33.1836
atom	O109	O_species	6.4062	3.1747	25.6247
atom	H110	H_species	5.3479	1.6063	25.5680
atom	H111	H_species	8.2203	2.7212	25.4168
atom	O112	O_species	11.1872	9.0140	6.7463
atom	H113	H_species	11.7919	9.1274	4.9511
atom	H114	H_species	9.2975	9.0707	6.7841

References

1. Hamann, D. R., Optimized norm-conserving Vanderbilt pseudopotentials. *Physical Review B* **2013**, *88* (8), 085117.
2. Nilsson, A.; Nordlund, D.; Waluyo, I.; Huang, N.; Ogasawara, H.; Kaya, S.; Bergmann, U.; Näslund, L. Å.; Öström, H.; Wernet, P.; Andersson, K. J.; Schiros, T.; Pettersson, L. G. M., X-ray absorption spectroscopy and X-ray Raman scattering of water and ice; an experimental view. *Journal of Electron Spectroscopy and Related Phenomena* **2010**, *177* (2), 99-129.
3. Fonseca Guerra, C.; Handgraaf, J. W.; Baerends, E. J.; Bickelhaupt, F. M., Voronoi deformation density (VDD) charges: Assessment of the Mulliken, Bader, Hirshfeld, Weinhold, and VDD methods for charge analysis. *Journal of computational chemistry* **2004**, *25* (2), 189-210.
4. Reeves, K. G.; Yao, Y.; Kanai, Y., Electronic stopping power in liquid water for protons and alpha particles from first principles. *Physical Review B* **2016**, *94* (4), 041108.
5. Schiwietz, G.; Grande, P., Improved charge-state formulas. *Nuclear Instruments and Methods in Physics Research Section B: Beam Interactions with Materials and Atoms* **2001**, *175*, 125-131.
6. Garcia-Molina, R.; Abril, I.; de Vera, P.; Kyriakou, I.; Emfietzoglou, D., A study of the energy deposition profile of proton beams in materials of hadron therapeutic interest. *Applied Radiation and Isotopes* **2014**, *83*, 109-114.
7. Penn, D. R., Electron mean-free-path calculations using a model dielectric function. *Physical Review B* **1987**, *35* (2), 482.
8. Emfietzoglou, D.; Garcia-Molina, R.; Kyriakou, I.; Abril, I.; Nikjoo, H., A dielectric response study of the electronic stopping power of liquid water for energetic protons and a new I-value for water. *Physics in Medicine & Biology* **2009**, *54* (11), 3451.
9. Ritchie, R., Energy losses by swift charged particles in the bulk and at the surface of condensed matter. *Nuclear Instruments and Methods In Physics Research* **1982**, *198* (1), 81-91.
10. Ashley, J., Optical-data model for the stopping power of condensed matter for protons and antiprotons. *Journal of Physics: Condensed Matter* **1991**, *3* (16), 2741.
11. Report 90. *Journal of the International Commission on Radiation Units and Measurements* **2014**, *14* (1), 34-37.